

Biological Durability, Cytotoxicity and MRI Image Contrast Effects of Chitosan Modified Magnetic Nanoparticles

The Tam Le¹, Hoa Du Nguyen¹, Thi Ngoc Linh Nguyen^{2,3}, Thien Vuong Nguyen^{3,4,*}, Phan Thi Hong Tuyet¹, Thi Hai Hoa Nguyen⁵, Quoc Thang Nguyen⁶, Thu Ha Hoang⁷, Tran Chien Dang⁸, Bui Le Minh⁹, Le Trong Lu^{3,4}, Duc Duong La¹⁰, Sheshanath V. Bhosale^{11,*}, and Dai Lam Tran^{3,4,*}

¹Vinh University, 182 Le Duan, Vinh City 460000, Vietnam

²Thai Nguyen University of Sciences, Thai Nguyen 250000, Vietnam

³Institute for Tropical Technology, Vietnam Academy of Science and Technology, Hanoi 100000, Vietnam

⁴Graduate University of Science and Technology, Vietnam Academy of Science and Technology, Hanoi 100000, Vietnam

⁵University of Science and Technology of Hanoi, VAST, Hanoi 100000, Vietnam

⁶Ha Tinh University, Ha Tinh City 480000, Vietnam

⁷University of Education, Vietnam National University, 144 Xuan Thuy, Cau Giay, Hanoi 100000, Vietnam

⁸Institute of Theoretical and Applied Research (ITAR), Duy Tan University, Hanoi 100000, Vietnam

⁹NTT Hi-Tech Institute, Nguyen Tat Thanh University, Ward 13, District 4, Ho Chi Minh City 700000, Vietnam

¹⁰Institute of Chemistry and Materials, Cau Giay, Hanoi 100000, Vietnam

¹¹School of Chemical Sciences, Goa University, Taleigao Plateau, Goa 403206, India

Delivered by Ingenta

In this manuscript, biological durability, cytotoxicity and MRI image contrast effect of chitosan modified magnetic nanoparticles were investigated. The result of durability study shows that the as-prepared sample with average size of about 30 nm had a high stability under pH conditions in range of from 2 to 12 and at salt concentration in range of from 0 to 300 mM. The cytotoxicity testing indicates that the obtained Fe₃O₄@CS ferrofluid revealed a low cytotoxicity. After 48 h of test on the line of prostate tumor cells of Sarcoma 180, collected IC₅₀ value was 178.5 ± 22 (μg/ml), 7.5 to 27.9 times less cytotoxicity than that of reported ferromagnetic fluids. MRI data shows that the transverse relaxation rate (*r*₂) of the ferrite nanoparticles was 130.32 (mM⁻¹s⁻¹), 2 and 1.44 times larger than that of the commercial products of Sinerem (AMI-227) and Ferumoxytol products, respectively. *In vivo* test in rabbit shows that the picture of body parts was clearly observed after the injection of the Fe₃O₄@CS ferrofluid. With these outstanding properties, this magnetic fluid based on the chitosan modified Fe₃O₄ nanoparticles had great potential for enhancing the image contrast in image diagnosis by MRI magnetic resonance imaging technique.

Keywords: Magnetic Resonance Imaging MRI, Cytotoxicity, Colloidal Stability, Chitosan, Magnetic Fluid.

1. INTRODUCTION

Magnetic Resonance Imaging (MRI) is a medical diagnostic technique that creates anatomical images of the body thank to using magnetic fields and radio waves. MRI is a non-interfering and non-irradiated imaging diagnostic technique so this method is highly safe for medical

purpose. However, the obtained signals are rather weak, which is difficult to detect tumors. In the clinical MRI research, the signal is determined based on the rest period of the hydrogen protons in the water molecule. In order to obtain better signal, several magnetic contrast drugs have been used to shorten the rest time of these protons. At the moment, the paramagnetic ionic complexes with large spin torque values like Gd³⁺ (having 7 unpaired

*Authors to whom correspondence should be addressed.

electrons) has been widely used as commercial T1 magnetic contrast drugs. Nine main derivatives of gadolinium used as contrast mediums includes gadobenic acid, gadobutrol, gadodiamid, gadofosveset, gadopentetic acid, gadoteric acid, gadoteridol, gadoversetamid and gadoxetic acid [3–10]. However, in recent years, side effects such as the risk of nephrogenic systemic fibrosis (NSF) caused by gadolinium drugs have been reported in many countries. The above symptoms were also detected on various organs such as liver, lungs and heart [3, 12]. The European Medicines Agency (EMA) has warned of the risk of nephrogenic systemic fibrosis relating to different gadolinium mixtures. US Food and Drug Administration (FDA) and European Society of Urogenital Radiology (ESUR) have also required manufacturers for providing the information about gadoliniums and their limited dose for high-risk patients on the label of the magnetic contrast drugs, and contraindicated the use of three gadolinium based magnetic contrast agents including Magnevist (gadopentate dimeglumine), Omniscan (gadodiamide) and Optimark (gadoversetamide) for patients with acute kidney injury, chronic kidney failure or severe kidney failure [10]. Canadian Medicines Agency (Health Canada) has also required for restricting the use in all eight gadoliniums based magnetic contrast drugs.

Recently, research and application of the magnetic nanoparticles as MRI image contrast drugs have been intensively reported for development of new magnetic contrast agents having lower cytotoxicity [41]. Compared with conventional MRI image contrast agents, the magnetic nanoparticles based drugs have many advantages: (i) stable and suitable complex groups for different biological objects; (ii) Different MRI contrast levels can be changed by controlling the shape, size and composition of the nanoparticles; (iii) The nanoparticles can form hybrid structures with antibodies or other biomolecules and through consolidation with these molecular probes, therefore it can product the multimodal MRI images; (iv) Ferromagnetic oxide (Fe_3O_4) based MRI contrast drugs can reduce T_2 and increase MRI recovery speech in weighted T_2 modes [2].

To be used as a drug for enhancing MRI image resonance, the magnetic nanoparticles must have sufficiently large magnetic saturation, superparamagnetic properties, relatively homogeneous and small size, good biological compatibility and low cytotoxicity [8, 27].

In order to enhance the biocompatibility, relaxivity and dispersion of the nanoparticles, their surface of magnetic nanoparticles were modified by some natural polymers such as chitosan (CS), agarose, saccharide, dextran [21, 27–38]. For examples, magnetic nanoparticles-immobilized agarose gels were successfully fabricated, which showed significant increase in relaxivity from $240 \text{ mM}^{-1}\text{s}^{-1}$ to $1000 \text{ mM}^{-1}\text{s}^{-1}$ with magnetic nanoparticles clusters immobilizing in a gel with

7% (w/w) [24]. In another study, Superparamagnetic iron oxide nanoparticles were immobilized with some saccharide derivative such as *N*-acetylglucosamine (GlcNAc) adduct into an *N*-acetyllactosamine adduct by *b*-1,4-galactosyltransferase [9]. These combinations showed enhanced MRI contrast with a variety of biofunctionalised surfaces.

However, it is of note that some factors such as the biological durability, control of polymer shell thickness [16], cytotoxicity [13], flocculation [23] and the elimination of the residual free polymers [42] and MRI contrast effect have not simultaneously investigated previously. Furthermore, no systematic studies on cytotoxic effects of MRI contrast agents and experimental data have been conducted long-term impact on the cells. Limited studies on *in-vivo* toxicity of magnetic liquid based on Fe_3O_4 were carried out and some others were incomplete. It is of note that several products have been reported innocuousness in *in-vivo* conditions while others have been shown the minimum toxicity in the same concentration [4, 36]. Thus, it is necessary to develop a new MRI image contrast drug with nanostructure, high colloidal stability, small size, low cytotoxicity and high magnetic saturation with systematically studies on its characteristics are necessary.

Herein, a magnetic fluid based on the chitosan-modified Fe_3O_4 nanoparticles is successfully fabricated. A systematically study on the biological durability, at various pH and salt concentrations, cytotoxicity is implemented, and *in-vitro* and *in-vivo* MRI image contrast tests of the magnetic fluid are also performed.

2. EXPERIMENTAL DETAILS

2.1. Chemicals

The analytical pure grade ferric chloride hexahydrate ($\text{FeCl}_3 \cdot 6\text{H}_2\text{O}$), ferrous chloride tetrahydrate ($\text{FeCl}_2 \cdot 4\text{H}_2\text{O}$) and sodium hydroxide were purchased from Merck chemical company. Ultra-pure nitrogen gas (99.99%) was used to provide anaerobic condition in solution. Distilled deionized water was used to prepare all the solutions. All chemicals were used as received without any further purification.

2.2. Synthesis of Fe_3O_4 @CS Magnetic Fluid

Superparamagnetic Fe_3O_4 nanoparticles were prepared by hydrothermal method following our previous work [39]. A mixture solution of ferrous and ferric chlorides at the molar ratio $\text{Fe(III)/Fe(II)} = 2$ was heated and kept at 75°C under N_2 flow and continuously stirred at 500 rpm/min for 20 min. This solution was then dripped into 15 ml sodium hydroxide solution (NaOH 3 M) under vigorous stirring and N_2 atmosphere for 1 hours. The mixture was then putted into a Teflon-lined stainless-steel hydrothermal reactor, heated and kept at 160°C for 3 hours. The obtained Fe_3O_4 nanoparticles were washed by centrifugation at 12,000 rpm/min for 5 min and decanted by the assistant of magnet. The as-prepared magnetic

nanoparticles (MNPs) were dispersed into chitosan solution at 70 °C by using a supersonic bath (Model TPC-25, Switzerland) for 30 min. The obtained chitosan coated MNPs ($\text{Fe}_3\text{O}_4@CS$) were then purified by centrifugation and dispersed in deionized water.

2.3. Characterization of Magnetic Nanoparticles

The phase structures of the samples were characterized by XRD using diffractometer D8 Advance Bruker with $\text{Cu-K}\alpha$ radiation ($\lambda = 1.5406 \text{ \AA}$). The chemical structures of chitosan on the surface of Fe_3O_4 nanoparticles was analyzed by FT-IR spectroscopy (Nicolet 6700). The amount of chitosan on the particle surface was determined by TGA analysis (Labsys 18TG/DSC Setaram). Morphology of the particles was obtained by transmission electron microscopy TEM (JEOL JEM 1010) and hysteresis loops were measured at room temperature to the highest field of 10 k by using a vibrating sample magnetometer (VSM).

The hydrodynamic size and colloidal stability of the magnetic fluids in different electrolyte and pH were measured by using dynamic light scattering (DLS) and zeta potential measurements (HORIBA SZ-100Z system) [20, 33].

The saturation magnetization of the samples at room temperature was measured under the highest magnetic field of 10 kOe by using a vibrating sample magnetometer (VSM) [26, 37].

2.4. In Vitro Cytotoxicity Study

2.4.1. Cell Culture

The Sarcoma 180 cells used in this study were provided from American Type Culture Collection then were cultured in RPMI 1640 medium, supplemented with 10% fetal bovine serum FBS; 1% combination of penicillin and streptomycin.

2.4.2. MTT Assay

To evaluate the effect of the nanoparticles on the viability of cells, MTT assay was performed according to Ref. [37]. After seeding 5×10^3 Sarcoma 180 cells per well in 96-well flat-bottomed microtiter plates, cells were incubated with 20 μl of diluted $\text{Fe}_3\text{O}_4@CS$ NPs to reach the concentration between 15.125 μM –125 μM for 48 hours. After that, 100 μl of the medium was removed before adding 20 μl of MTT solution and incubated for 4 hours at room temperature. Under the metabolism activity of viable cells, the MTT was taken into mitochondria and changed into blue formazan crystals. A microplate reader was used to measure the absorbance at 490 nm and all values were performed as a percentage of the control. Graph and inhibitory concentration IC50 value was obtained by using Microsoft Excel. All presented values were expressed as mean \pm standard deviation (SD).

2.5. MRI measurements

2.5.1. Preparation

Diluted sets of the sample from 10–60 $\mu\text{g/ml}$ (as elemental iron) of formulations were prepared with 10 $\mu\text{g/ml}$, 15 $\mu\text{g/ml}$, 30 $\mu\text{g/ml}$, 45 $\mu\text{g/ml}$ and 60 $\mu\text{g/ml}$ and placed in 2 ml vials. Dilution was performed after 2 min vortex of the 5 mg/ml stock solutions.

2.5.2. Imaging

MRI contrast effects of $\text{Fe}_3\text{O}_4@CS$ solutions were performed by using a 1.5 T MRI scanner (SIEMENS MAGNETOM, Germany). The value of reflexivity r_2 was measured with a multi-echo spin-echo sequence with TR fixed. Syngo@fastView and EFilm Workstation (Merge Healthcare) softwares were used to draw regions of interest (ROIs) and calculate the relaxation rate. Transversal relaxation rates ($1/T_2$ or R_2 , s^{-1}) were plotted as a function of iron concentration, expressed in mM of iron, and the transverse (r_2) relativity was obtained by the slope of the fitting straight line. Decay curves were fitted with a mono-exponential decay equation to calculate T_2 , where A is the absolute bias and C is the signal intensity T_2 of the samples, which was measured using the Multi-Slice Multi-Echo (MSME) pulse sequence with the following parameters: effective TE, with 09 echoes ranging from 12 to 112 ms, TR = 4000 ms, $181 \times 200 \text{ mm}^2$ $x - y$ field of view (FOV), 3 mm slice thickness, 343×512 matrix size providing $200 \mu\text{m}^2$ $x - y$ resolution, number of averages = 2, total acquisition time = 46 min 09 s for rabbit imaging.

3. RESULTS AND DISCUSSION

The average size of nanoparticles was analyzed using Image software and their schematic illustration of the morphology. Figure 1 exhibits the characterization of obtained $\text{Fe}_3\text{O}_4@CS$ nanoparticles.

As can be seen in Figure 1(a), all the characteristic peaks were consistent with the standard database peaks, revealing the cubic inverse spinel structure of the sample. The Figure 1(b) illustrates the FTIR spectra of Fe_3O_4 (red line), chitosan (blue line), and chitosan-coated Fe_3O_4 (black line). It can be seen that the FTIR spectrum of Fe_3O_4 shows a strong peak at 586 cm^{-1} , which is assigned to the characteristic Fe–O stretching vibration of magnetic nanoparticles [19]. The vibration peak at 459 cm^{-1} is attributed to tetrahedral and octahedral sites and peaks at 3400 cm^{-1} assigned to the O–H stretching from absorbed moisture on the surface of the magnetic particles [43]. In the FTIR spectrum of chitosan, the absorption bands at 2920, 1415, and 1067 cm^{-1} are attributed to the stretching vibrations of C–H, C–N, and C–O, respectively, and the band 1640 cm^{-1} is due to the bending vibration of $-\text{NH}_2$. In case of chitosan-coated Fe_3O_4 nanoparticles, the FITR shows all the characteristic vibrations of both Fe_3O_4 and chitosan. The shifts in the position of peaks at 1640 and 590 cm^{-1} demonstrate that the existence of a

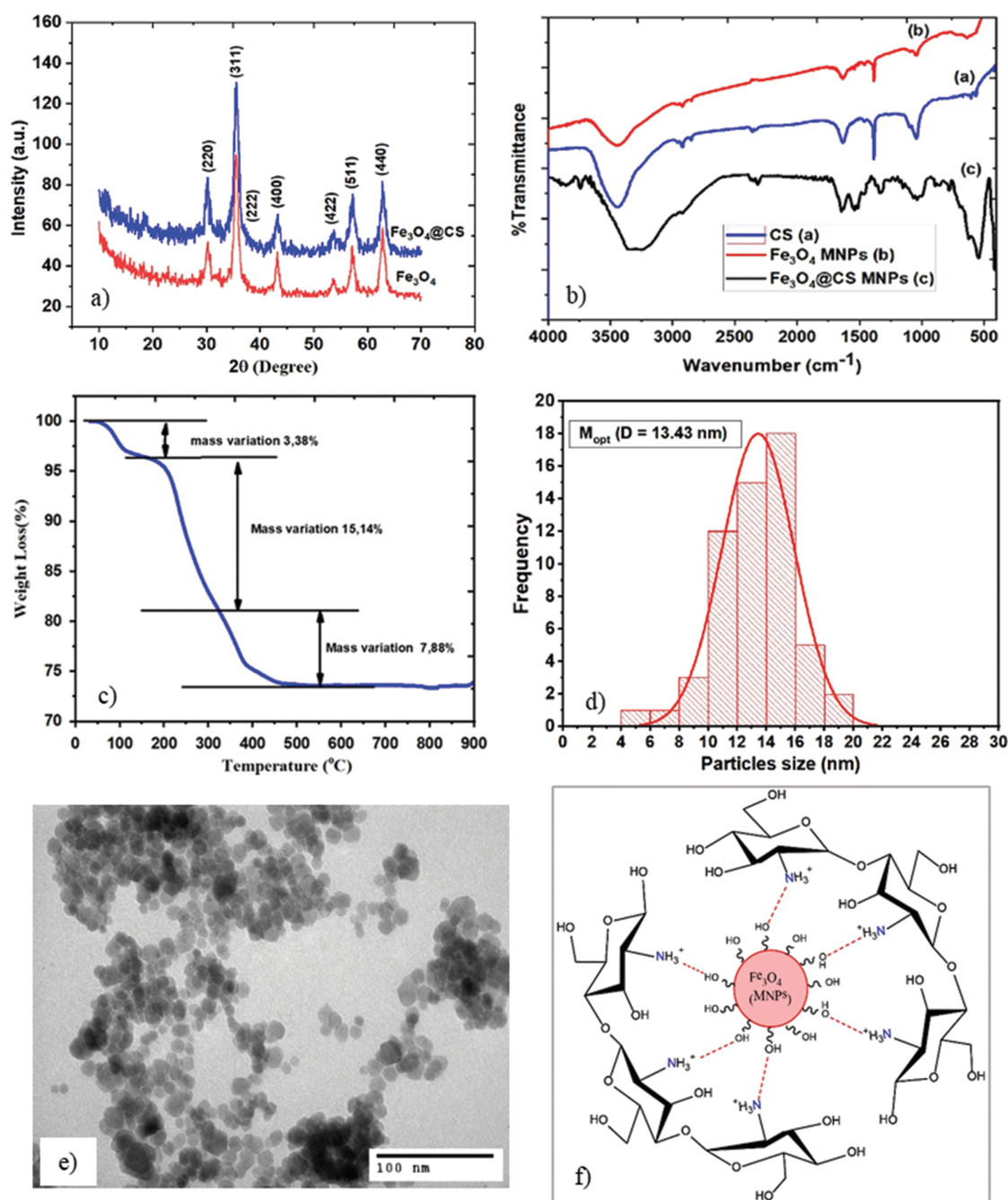


Figure 1. Powder X-ray diffraction of the Fe_3O_4 , Fe_3O_4 @CS (a); FT-IR spectra for pure chitosan, bare ferrite particles, and chitosan-coated Fe_3O_4 MNPs (b); TGA analysis of Fe_3O_4 @CS NPs (c); the size distribution histograms of the Fe_3O_4 @CS MNPs (d); their TEM photographs (e) and their schematic illustration of the morphology (f).

hydrogen bond between the surface oxygen of Fe_3O_4 and the hydrogen of the amino group ($-\text{NH}_2$) in the chitosan. The broadening of the band at 3400 cm^{-1} may be due to the interaction between OH on surface of Fe_3O_4 and $-\text{NH}_2$ of CS and the present of OH groups of CS layer. The thermogravimetric analysis (TGA) curve of the Fe_3O_4 @CS MNPs (Fig. 1(c)) shows the weight loss of 23% at temperature range from 200 to 550 °C were the amount of

chitosan on the surface of the Fe_3O_4 @CS MNPs. The TEM image indicate that the shape of the Fe_3O_4 @CS MNPs were spherical and relatively uniform with the mean size of 13.43 nm. Since the particles size observed in TEM is less than 100 nm. The Debye–Scherrer equation can be also employed to determine average crystal size:

$$d = \frac{K\lambda}{B \cos \theta}$$

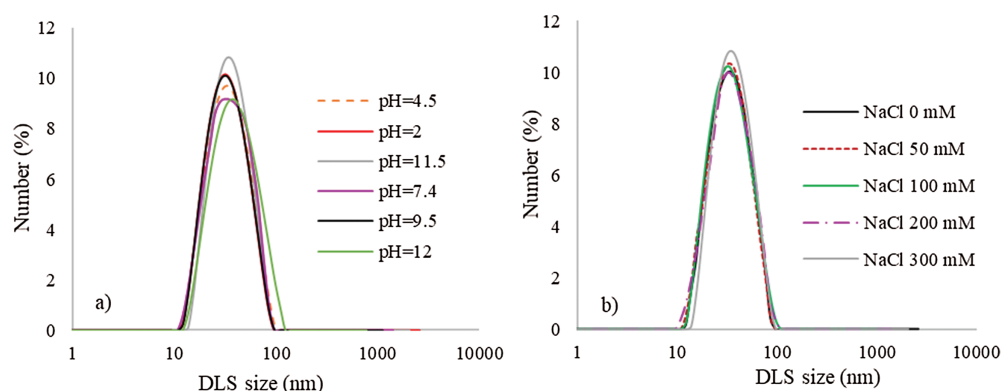


Figure 2. Hydrodynamic size distribution of the Fe_3O_4 @CS magnetic fluid at different pHs (a) and at different NaCl concentrations (b).

where K is a constant dependent on the crystallite shape, θ is the degree (position of the peak), λ is the X-ray wavelength, and B represents the full width at half maximum (FWHM) of the peak. The average crystal size calculated from Debye–Scherrer equation is approximately 13 nm, which is consistent with particle sized obtained from TEM study.

In order to utilize as biomedical material, magnetic nanoparticles should be well-dispersed and long-term stable in aqueous solution. The colloidal stability of the nanoparticles depends on several parameters such as the particle size, hydrophilic or hydrophobic functional groups on the surface of the nanoparticles. Under biological conditions, the colloidal nanoparticles stability depends on several factors such as salt, interactions between proteins and especially, enzymes activity. While the interaction between the nanoparticles and biomolecular complexes entities are difficult to evaluate, the influence of salt concentration and pH on the colloidal stability of the nanoparticles was selected to investigate the biomedical application ability of the nanoparticles. In this study, the dispersity of Fe_3O_4 @CS nanoparticles was examined by DLS and zeta potential measurements. It is well known that salt concentration in the body is maintained at about 158 mM, and the pH value is around 7.3. In the current study, the colloidal stability of the Fe_3O_4 @CS nanoparticles in saline at the concentrations in the range from 0–300 mM and the pH value from 2 to 12 were evaluated. Obtained results is presented in Figure 2.

As can be seen from Figure 2, when the pH value varied from 2 to 12, the hydrodynamic size of the Fe_3O_4 @CS nanoparticles maintained about 28 nm. This indicates that the nanoparticles dispersed well and were stable in studied solution. Similarly, when the NaCl concentration increased from 0 to 300 mM, the hydrodynamic size also remained about 30 nm. This suggests that the sample was stable under the studied saline condition.

The long-term colloidal stability of the Fe_3O_4 @CS magnetic fluid was evaluated using the zeta-potential which is a measurement of the surface charge on the nanoparticles in aqueous solutions. The zeta potential scanning of

the Fe_3O_4 @CS magnetic fluids initial and after 90 days of storage is shown in Figure 3. It can be clearly seen that the chitosan-coated Fe_3O_4 nanoparticles have a wide (absolute) range of the zeta-potential values. the chitosan-coated Fe_3O_4 nanoparticles has a positive charge of about 45 mV, which is large enough to prevent the particles form aggregations by electrostatic repulsion [17]. This zeta-potential value is extremely stable as after 90 days of storage, only 1 mV in decrease of zeta-potential value is observed. This result indicates that the prepared chitosan-coated Fe_3O_4 nanoparticles are highly stable in the aqueous solution in a long period of time.

Result of the magnetization-magnetic field strength (M–H) measurement at room temperature is presented in Figure 4. This figure shows that the small coercivity and low magnetic remanence which were about 6 Oe and 0.3 emu/g, respectively. Furthermore, the hysteresis loops are fitted well in the Langevin function:

$$M = n\mu L\left(\frac{\mu H}{kT}\right) = n\mu \left[\coth\left(\frac{\mu H}{kT}\right) - \frac{kT}{\mu H} \right]$$

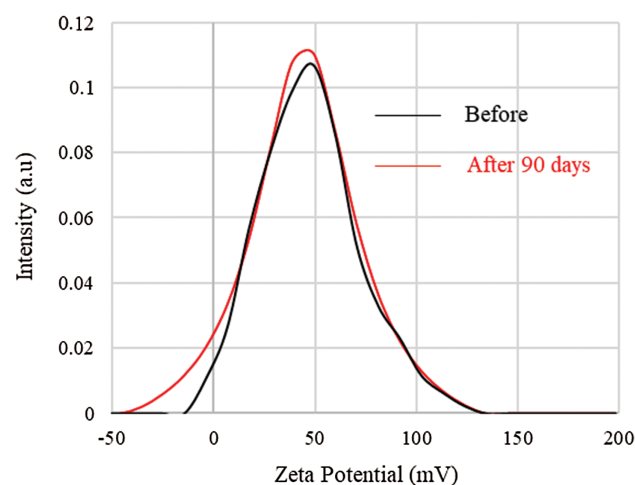


Figure 3. Zeta potential scanning of the Fe_3O_4 @CS magnetic fluids initial and after 90 days of storage.

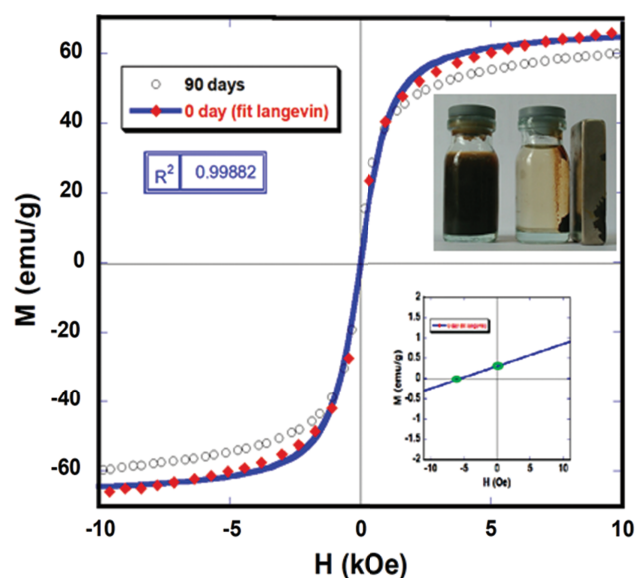


Figure 4. Experimental and fitting hysteresis curves of the $\text{Fe}_3\text{O}_4@CS$ nanoparticles (inset is the enlarged hysteresis curve).

with $R^2 > 0,998$. This indicates that the obtained $\text{Fe}_3\text{O}_4@CS$ nanoparticles were superparamagnetic materials at room temperature [40]. The saturation magnetization of the material was 68 emu/g.

MTT assay was done on Sarcoma 180 cell lines to examine the cytotoxicity effect of the $\text{Fe}_3\text{O}_4@CS$ MNPs on mammalian cells. This assay is based on the metabolic activity of living cells which cleavages a soluble tetrazolium (yellow) into insoluble formazan (purple). It has been demonstrated that the level of formazan crystal creation is proportional to the cell viability. The IC_{50} value was calculated from the cell viability-concentration curve in terms of absorbance. Obtained MTT result is exhibited in Figure 5.

As can be seen from Figure 5, the $\text{Fe}_3\text{O}_4@CS$ MNPs revealed a low cytotoxicity on Sarcoma 180 with the cell viability of 106–83% in the range of the MNP concentration from 15.125 $\mu\text{g}/\text{ml}$ to 62.5 $\mu\text{g}/\text{ml}$. When increase of the MNPs concentration to 125 $\mu\text{g}/\text{ml}$, survival cell rate reduced to 66.1%. The low survival cell rate at the high MNPs concentration is possibly resulted from the MNP-induced stress, which under the “overload dose,” the outer layer of the MNPs around the cells would block the entering of nutrient and dissolve gases such as oxygen [25]. The IC_{50} value of the $\text{Fe}_3\text{O}_4@CS$ MNPs on Sarcoma 180 calculated after 48 hours was 178.5 ± 22 ($\mu\text{g}/\text{ml}$). Obtained results indicate that the $\text{Fe}_3\text{O}_4@CS$ MNPs cause insignificant toxic effect on the Sarcoma 180 cell line.

Morphology of cells observed by using an inverted microscope is presented in Figure 6. This figure shows that the morphology of cells was insignificantly influenced by the presence of the $\text{Fe}_3\text{O}_4@CS$ MNPs. At the highest concentration (125 $\mu\text{g}/\text{ml}$), the $\text{Fe}_3\text{O}_4@CS$ MNPs were aggregated and formed a thin layer on the surface of the

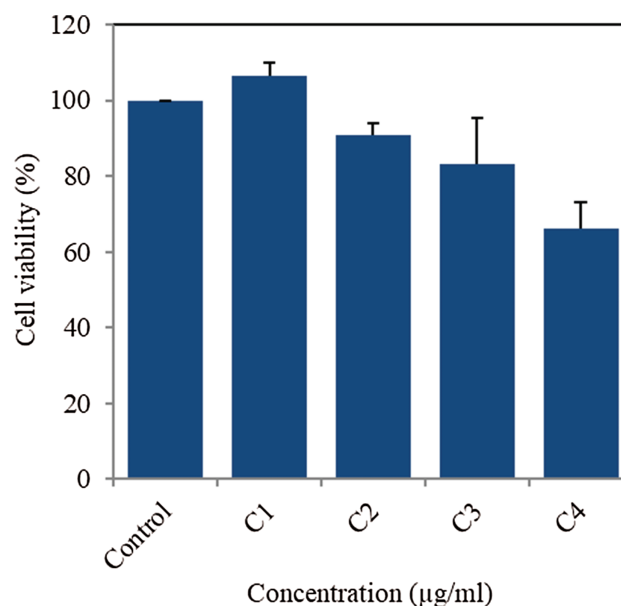


Figure 5. Sarcoma 180 cell's viability incubating with $\text{Fe}_3\text{O}_4@CS$ MNPs at different concentrations: 15,125 $\mu\text{g}/\text{ml}$ (C1), 30,25 $\mu\text{g}/\text{ml}$ (C2), 62,5 $\mu\text{g}/\text{ml}$ (C3) and 125 $\mu\text{g}/\text{ml}$ (C4) after 48 h.

cells. However, the morphology of cells (spherical shape) were unchanged, which confirms the low cytotoxicity of the $\text{Fe}_3\text{O}_4@CS$ MNPs.

The as-synthesized $\text{Fe}_3\text{O}_4@CS$ MNPs in this work exhibited a lower cytotoxicity compared with other published superparamagnetic iron oxide nanoparticles. Previous studies on HeLa cells (human cervix carcinoma), HepG₂ cells (human liver cancer), MCF-7 (human breast cancer) and Jurkat cells (human leukemia) indicated that the IC_{50} values of magnetic iron oxide nanoparticles were 12.5 ± 1.7 , 23.83 ± 1.1 , 18.75 ± 2.1 and 6.4 ± 2.3 ($\mu\text{g}/\text{ml}$), respectively, so our sample had about 7.5–27.9 times less cytotoxicity. Another study on CHO-K1 cells (Chinese Hamster ovaries) also indicated that a sample of iron oxide nanoparticles had higher toxicity on human cancer cell lines. Their IC_{50} was less than 100 $\mu\text{g}/\text{ml}$ after 72 h of cell exposure [11]. In the same way, Ferucarbotran (Resovist[®]), an approved superparamagnetic iron oxide contrast agent for MRI, reduced cell viability of human aortic endothelial cells to 63% after 48 h at the concentration of 50 $\mu\text{g Fe}/\text{ml}$ [15]. The lower toxicity of our $\text{Fe}_3\text{O}_4@CS$ MNPs was possible due to the small size of the nanoparticles (13.4 nm for the inorganic core and about 28 nm for the core/shell, DLS size) and due to the present of CS layer. It was explained that the small nanoparticles could pass through the cell membrane thank to the interaction between negative charged domain on cell membranes and the amino groups of chitosan [30]. The NPs would then induce ROS (reactive oxygen species) and lysosomal and mitochondrial damage [22]. On the other hand, the low toxicity of the as-synthesized $\text{Fe}_3\text{O}_4@CS$ NPs indicated that the chitosan

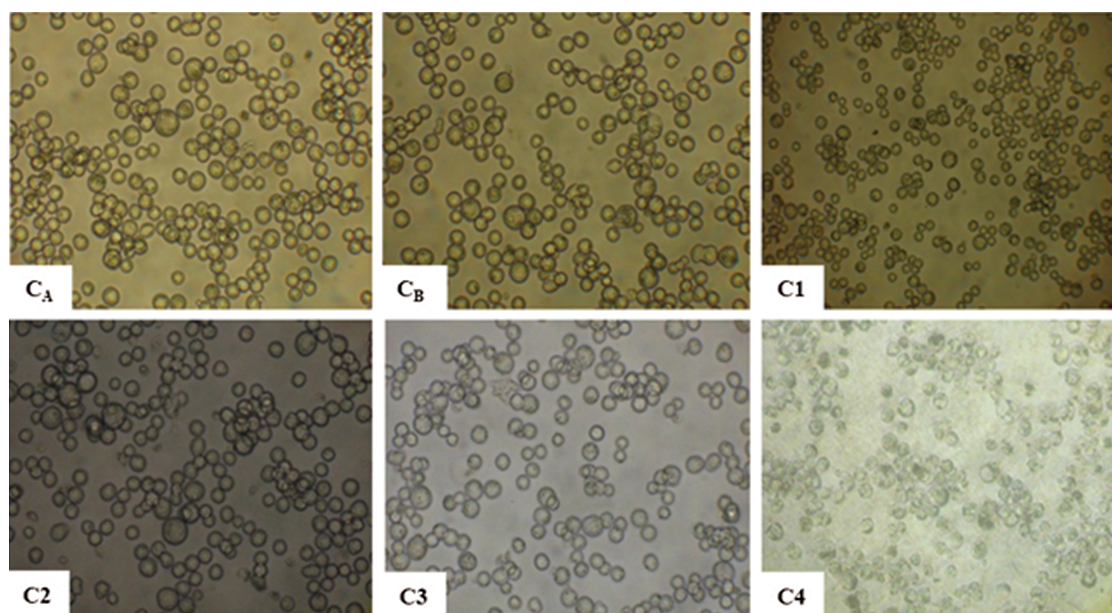


Figure 6. Inverted microscope images of Sar.180 cells in the presence of the $\text{Fe}_3\text{O}_4@CS$ MNPs at the different concentrations. Control with culture medium (C_A), Control with DMSO (C_B), $\text{Fe}_3\text{O}_4@CS$ concentration: 15,125 $\mu\text{g/ml}$ (C_1), 30,25 $\mu\text{g/ml}$ (C_2), 62,5 $\mu\text{g/ml}$ (C_3) and 125 $\mu\text{g/ml}$ (C_4). Objective lens: 20 \times , Zoom: 5.6.

oligosaccharide coating decreased significantly the cytotoxic impact of the nanoparticles [29]. Other classical group that is gadolinium-based contrast agents such as Magnevist[®], Dotarem[®] or Omniscan[®] were approved by the U.S. Food and Drug Administration (FDA) as MRI contrast agents but since 2010, FDA changed the drug label for those based on the risk of causing nephrogenic systemic fibrosis in patients with kidney dysfunction. Furthermore, in 2017 the Pharmacovigilance Risk Assessment Committee (PRAC) announced about the potential risks of using these products due to their accumulation in the brain and other tissues. Therefore, biocompatibility is a key property of Fe_3O_4 NPs, the $\text{Fe}_3\text{O}_4@CS$ NPs from this work is expected to overcome the available disadvantages of published products, reduce the systemic toxicity and have long blood circulation to improve the target capacity while applied as either drug delivery or diagnosis agent. In a previous work, CS nanoparticles exhibited very impressive antitumor efficacy *in vivo* against S-180 [1] (Qi and Xu, 2006). In addition, the low cytotoxicity of our $\text{Fe}_3\text{O}_4@CS$ NPs suggested that the chitosan oligosaccharide coating layer improved significantly the non-cytotoxicity of the sample, and thus the as-prepared $\text{Fe}_3\text{O}_4@CS$ MNPs were expected to reduce the systemic toxicity and have potential for clinical applications.

In-vitro MR imaging using $\text{Fe}_3\text{O}_4@CS$ MNPs as contrast agent and the transverse relaxation rate r_2 are presented in Figure 7. As can be seen from Figure 7, the $\text{Fe}_3\text{O}_4@CS$ MNPs exhibited an increase of the transverse relaxation rate r_2 and acted as contrast agents in the MR imaging, which showed a signal loss (darker) contrast on the r_2 value or the T_2 -weighted MR images.

The signal intensity of MRI and MRI contrast effect of the $\text{Fe}_3\text{O}_4@CS$ MNPs were clearly changed according to their concentration (Fig. 7(a)).

On the Multi-Slice Multi-Echo (MSME) image, the echo time (TE) was used to control the image contrast and the “weighting” of the T_2 image. The overall signal intensity (S) of a MSME sequence can be approximately expressed:

$$S = K \cdot [H] \cdot (1 - e^{-TR/T_1}) \cdot e^{-TE/T_2}$$

When the TE reduced, the TE/T_2 ratio decreased toward zero, the T_2 -weighting term e^{-TE/T_2} reached to 1. Conversely, the importance of the exponential weighting term increased when TE was extended compared with T_2 , and so “ T_2 -weighting” was higher. To evaluate systematically the T_2 -weighted MRI images, the experiment was carried out at different values of TE.

Figure 7(b) shows the T_2 -weighted MRI images at the different concentrations of the MNPs and various values of TE. As can be seen from the Figure 7(b), the MRI signal intensity increased with increasing the nanoparticles concentrations and TE values. Data from Figures 7(d) and (e) showed that even when TE of 37 ms, the change in signal intensity was large enough in comparison with control sample. In medical practice, with TE of 50 ms or higher was usually applied for MRI measurements. With smaller TE values, the time needed to collect signal was shorter and the images were sharper.

In the color map of r_2 value coded image, positive and negative contrasts were indicated by the bright violet and orange color, respectively. In the Figure 7(f), the transverse relaxation rate r_2 of the $\text{Fe}_3\text{O}_4@CS$ nanoparticles

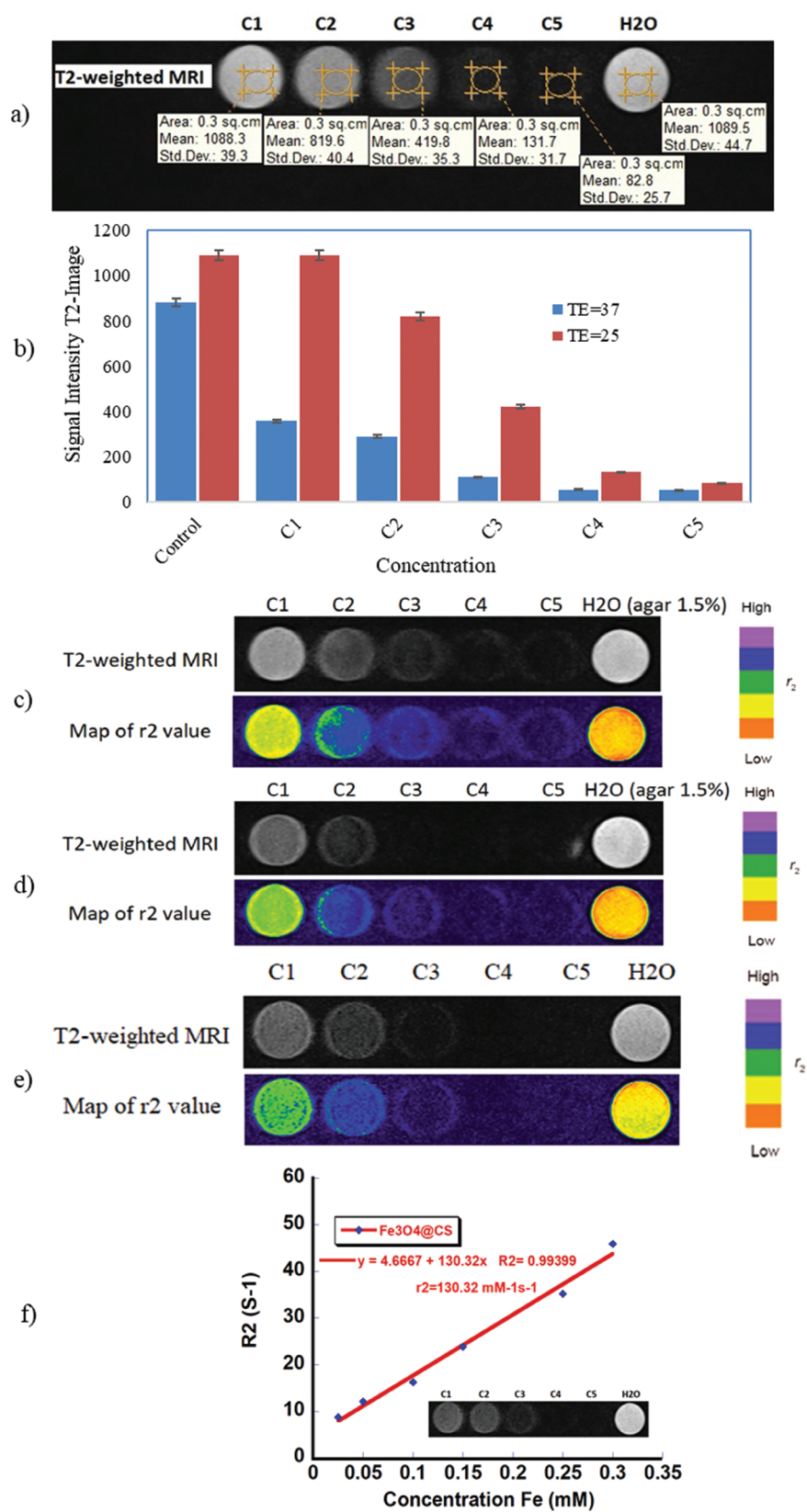


Figure 7. The signal intensity of MRI and MRI contrast effect of the $\text{Fe}_3\text{O}_4@CS$ MNPs (a); the MRI signal intensity at the different concentrations of the MNPs and at the different values of TE (b); T_2 -weighted contrasts and r_2 color maps in the presence of the $\text{Fe}_3\text{O}_4@CS$ nanoparticles at the different concentrations in 1.5% agarose solution: TR = 4000 ms, TE = 25 (c); TE = 37 ms (d) and TE = 50 ms (e); $1/T_2$ (R_2)-Fe concentration plot of the $\text{Fe}_3\text{O}_4@CS$ nanoparticles at 1.5 T (f).

Table I. Relaxation rate r_2 of Fe_3O_4 @CS and commercial Fe_3O_4 nanoparticle-based MRI contrast agents at 37 °C

Brand name	Ligand shell	DLS size (nm)	r_2 relaxation rate ($\text{mM}^{-1}\text{s}^{-1}$)/T	Target	Company
Ferumoxides (Feridex IV, Endorem)	Dextran	80–150	120, 1.5T	Reticuloendothelial System, Liver Stem cell labeling	Advanced magnetics (U.S.A)
AMI-25, Feridex	Dextran	58	107, 0.47T		
Sinerem (AMI-227)	Dextran	15–30	65, 1.5T	Blood pool	Guerbet (France)
Ferumoxytol	Carboxymethyl-dextran	30	89, 1.5T	Macrophage Blood pool	Advanced magnetics (U.S.A)
VSOP-C184 ferropharm	Citrate	7	33.4, 1.5T	–	Guerbet, advanced magnetics
Ferucarbotran (SHU-555A), resovist	Carboxydextran	60	189, 1.5T	Liver	Bayer schering (Germany)
MION-46L	Dextran	18–24	35, 0.47T	Liver	Center for molecular imaging Research, charlestown, MA
SHU-555C ferucarbotran, supravist	Dextran	20	90, 1.5T	Blood pool	Bayer schering (Germany)
Fe_3O_4 @CS	Chitosan	28–30	130.32, 1.5 T	–	Current study

in agar. of 1.5%, which was determined by taking the slope of a linear fit of $1/T_2$ versus the Fe concentration, was 130.32 ($\text{mM}^{-1}\text{s}^{-1}$). This r_2 value was larger than that of the major commercial Fe_3O_4 products such as Ferumoxide (Feridex) [18], AMI-25 (Feridex; Endorem) and MION [14], SHU 555C (Supravist) [34] and larger than that reported by Cha [4]. The transverse relaxation rate r_2 of the Fe_3O_4 @CS nanoparticles were smaller than that of SHU-555A (Ferucarbotran) (Table I). This is ascribed to the high r_2 value of the prepared Fe_3O_4 @CS MNPs in this work leading to the high saturation magnetizations value of Fe_3O_4 cores (68 emu/g), which decrease the transverse relaxation rate r_2 .

To evaluate the clinical imaging application potential of the Fe_3O_4 @CS MNPs, *in vivo* experiment on a rabbit weighting 1.5 kg was carried out. For MRI imaging, 3 ml of Fe_3O_4 @CS MNPs solution (at concentration of 5 mg/ml) was injected in the rabbit via ear vein (Fig. 8). MR images in T_2 mode showed a sharp contrast MR images compared to before the injection. Specifically, after 15 min of the injection (Fig. 8(b)), spleen, liver and kidney were more clearly observed than before the

injection (Fig. 8(a)). In this figure, the liver part of the image was darker than the image before the injection. Especially, when getting 0.3 cm^2 liver tissue before and after injecting Fe_3O_4 @CS, the signal strength diminished from 185.3 to 84 pixel (in proportion to 2.2 times to before injecting) and is showed on Figure 8. The results of animal experimentation show that the contrast agent based on our Fe_3O_4 @CS nanoparticles can be used as a T_2 agent in MRI.

Superparamagnetic iron oxide nanoparticles (SPIOs) injecting vein was an effective contrast agent for magnetic resonance imaging (MRI). SPIOs were phagocytosed by macrophages in different target tissues depending on the particle size and their composition [5, 32, 35]. For SPIOs having a relatively large hydrodynamic (DLS) size of 50 to 100 nm quickly implemented by macrophages of the reticule-endothelial system (RES) such as liver, spleen and bone marrow and failed tumor-associated macrophages (TAMs) *in vivo*, while ultrasmall superparamagnetic iron oxide nanoparticles (USPIOs) with hydrodynamic sizes below 50 nm would escape from RES phagocyte into some

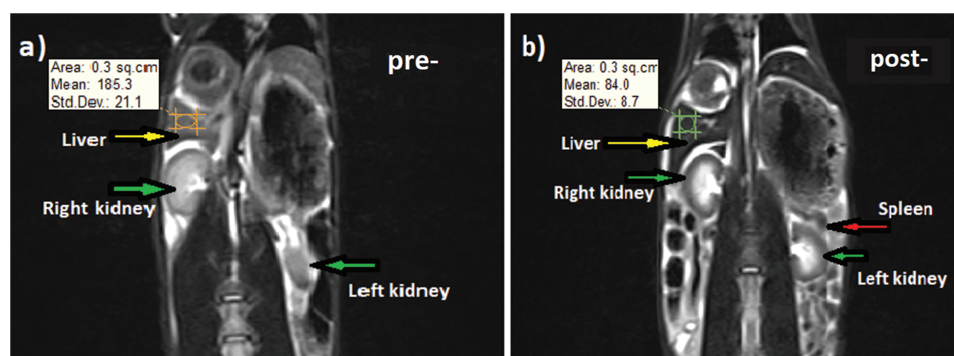


Figure 8. T_2 -weighted MR images of the liver, kidney, spleen of a rabbit: Before (a) and after 15 minutes (b) of the injection of the Fe_3O_4 @CS ferrofluid.

extent, leading to prolonged circulation and accumulated in blood in tissues and tumors that were inflamed due to trans endothelial leak and macrophage phagocytosis [6, 7]. Based on these results, we believed that for “*in vivo* tumor-associated macrophages labeling,” the Fe₃O₄@CS ferrofluid obtained with hydrodynamic size about 30 nm are advantageous in tumor accurate diagnosis, thank to escape of the Fe₃O₄@CS ferrofluid from Reticuloendothelial system.

4. CONCLUSIONS

In summary, biological durability, cytotoxicity, magnetic properties and MRI image contrast ability of Fe₃O₄@CS magnetic liquid were studied. The results of durability studies showed that the as-prepared sample had high stability under pH conditions in ranging from 2 to 12 and salt concentrations from 50 to 300 mM with dynamic size values DLS of from 28–30 nm. The results of toxicity tests found that the Fe₃O₄@CS magnetic liquid had a low cytotoxicity. On the line of prostate tumor cells of Sarcoma 180 test, after 48 hours, collected IC₅₀ value was 178.5 ± 22 (μg/ml), 7.5 to 27.9 times less toxicity than that of published ferromagnetic nanoparticles. *In-vitro* MRI imaging result data showed that the transverse relaxation rate (*r*2) was high (130.32 mM⁻¹s⁻¹). *In-vivo* test results in rabbits show that the image of body parts was clearly observed after the injection of the Fe₃O₄@CS ferrofluid. This magnetic fluid based on the chitosan-modified Fe₃O₄ nanoparticle had great potential to be used as a drug to enhance image contrast in image diagnosis by MRI magnetic resonance imaging technique.

Acknowledgments: This work is financially supported by MOET grant # B2019-TDV-03 (Le The Tam) and B2018-HHT-05. S.V.B. (GU) University Grant Commission (UGC) Faculty Research Program, New Delhi, India for an award of Professorship and also acknowledges Council of Scientific and Industrial Research (CSIR), India for providing support, code No. 02(0357)/19/EMR-II.

References and Notes

- Adhikari, H.S. and Yadav, P.N., **2018**. Anticancer activity of chitosan, chitosan derivatives, and their mechanism of action. *International Journal of Biomaterials*, *2018*, pp.1–29.
- Ali, L.M., Marzola, P., Nicolato, E., Fiorini, S., Guillamón, M.D.L.H., Piñol, R., Gabilondo, L., Millán, A. and Palacio, F., **2019**. Polymer-coated superparamagnetic iron oxide nanoparticles as T2 contrast agent for MRI and their uptake in liver. *Future Science OA*, p.FSO235.
- Caravan, P., Ellison, J.J., McMurry, T.J. and Lauffer, R.B., **1999**. Gadolinium (III) chelates as MRI contrast agents: Structure, dynamics, and applications. *Chemical Reviews*, *99*(9), pp.2293–2352.
- Cha, R., Li, J., Liu, Y., Zhang, Y., Xie, Q. and Zhang, M., **2017**. Fe₃O₄ nanoparticles modified by CD-containing star polymer for MRI and drug delivery. *Colloids and Surfaces. B: Biointerfaces*, *158*, pp.213–221.
- Corot, C., Robert, P., Idée, J.-M. and Port, M., **2006**. Recent advances in iron oxide nanocrystal technology for medical imaging. *Advanced Drug Delivery Reviews*, *58*(14), pp.1471–1504.
- Daldrup-Link, H.E., Rydland, J., Helbich, T.H., Bjørnerud, A., Turetschek, K., Kvistad, K.A., Kaindl, E., Link, T.M., Staudacher, K. and Shames, D., **2003**. Quantification of breast tumor microvascular permeability with feruglose-enhanced MR imaging: Initial phase II multicenter trial. *Radiology*, *229*(3), pp.885–892.
- Daldrup-Link, H.E., Simon, G.H. and Brasch, R.C., **2006**. Imaging of tumor angiogenesis: Current approaches and future prospects. *Current Pharmaceutical Design*, *12*(21), pp.2661–2672.
- Du, Y., Liu, X., Liang, Q., Liang, X.-J. and Tian, J., **2019**. Optimization and design of magnetic ferrite nanoparticles with uniform tumor distribution for highly sensitive MRI/MPI performance and improved magnetic hyperthermia therapy. *Nano Letters*, *19*(6), pp.3618–3626.
- Fallows, T.W., Mcgrath, A.J., Silva, J., Mcadams, S.G., Marchesi, A., Tuna, F., Flitsch, S.L., Tilley, R.D. and webb, S.J. **2019**. High-throughput chemical and chemoenzymatic approaches to saccharide-coated magnetic nanoparticles for MRI. *Nanoscale Advances*, *1*, pp.3597–3606.
- Gao, L., Zhou, J., Yu, J., Li, Q., Liu, X., Sun, L., Peng, T., Wang, J., Zhu, J. and Sun, J., **2017**. A novel Gd-DTPA-conjugated Poly (L-γ-glutamyl-glutamine)-paclitaxel polymeric delivery system for tumor theranostics. *Scientific Reports*, *7*(3799), pp.1–13.
- Hanot, C., Choi, Y., Anani, T., Soundarrajan, D. and David, A., **2015**. Effects of iron-oxide nanoparticle surface chemistry on uptake kinetics and cytotoxicity in CHO-K1 cells. *International Journal of Molecular Sciences*, *17*(1), p.54.
- Hermann, P., Kotek, J., Kubíček, V. and Lukeš, I., **2008**. Gadolinium (III) complexes as MRI contrast agents: Ligand design and properties of the complexes. *Dalton Transactions*, *23*, pp.3027–3047.
- Juang, J.-H., Wang, J.-J., Shen, C.-R., Kuo, C.-H., Chien, Y.-W., Kuo, H.-Y., Tsai, Z.-T. and Yen, T.-C., **2010**. Magnetic resonance imaging of transplanted mouse islets labeled with chitosan-coated superparamagnetic iron oxide nanoparticles. *Transplantation Proceedings*, *42*(6), pp.2104–2108.
- Jun, Y.W., Lee, J.H. and Cheon, J., **2008**. Chemical design of nanoparticle probes for high-performance magnetic resonance imaging. *Angewandte Chemie International Edition*, *47*(28), pp.5122–5135.
- Kim, E., Kim, J.M., Kim, L., Choi, S.J., Park, I.S., Han, J.Y., Chu, Y. C., Choi, E.S., Na, K. and Hong, S.-S., **2016**. The effect of neutral-surface iron oxide nanoparticles on cellular uptake and signaling pathways. *International Journal of Nanomedicine*, *11*, pp.4595–4607.
- Kircher, M.F., Mahmood, U., King, R.S., Weissleder, R. and Josephson, L., **2003**. A multimodal nanoparticle for preoperative magnetic resonance imaging and intraoperative optical brain tumor delineation. *Cancer Research*, *63*(23), pp.8122–8125.
- Kuang, Y., Yuan, T., Zhang, Z., Li, M. and Yang, Y., **2012**. Application of ferriferrous oxide modified by chitosan in gene delivery. *Journal of Drug Delivery*, *2012*, pp.1–7.
- Lee, N. and Hyeon, T., **2012**. Designed synthesis of uniformly sized iron oxide nanoparticles for efficient magnetic resonance imaging contrast agents. *Chemical Society Reviews*, *41*(7), pp.2575–2589.
- Li, S., Zhang, T., Tang, R., Qiu, H., Wang, C. and Zhou, Z., **2015**. Solvothermal synthesis and characterization of monodisperse superparamagnetic iron oxide nanoparticles. *Journal of Magnetism and Magnetic Materials*, *379*, pp.226–231.
- Long, J., Fernig, D.G. and Thanh, N.T.K., **2009**. Facile synthesis of stable, water-soluble magnetic CoPt hollow nanostructures assisted by multi-thiol ligands. *Journal of Material Chemistry*, *19*, pp.6023–6028.
- Luchini, A., Heenan, R.K., Paduano, L. and Vitiello, G., **2016**. Functionalized SPIONs: The surfactant nature modulates the self-assembly and cluster formation. *Physical Chemistry Chemical Physics*, *18*(27), pp.18441–18449.

22. Mahmoudi, M., Laurent, S., Shokrgozar, M.A. and Hosseinkhani, M., **2011**. Toxicity evaluations of superparamagnetic iron oxide nanoparticles: Cell "vision" versus physicochemical properties of nanoparticles. *American Chemical Society Nano*, 5(9), pp.7263–7276.
23. Mccarthy, J.R. and Weissleder, R., **2008**. Multifunctional magnetic nanoparticles for targeted imaging and therapy. *Advanced Drug Delivery Reviews*, 60(11), pp.1241–1251.
24. Mues, B., Buhl, E.M., Schmitz-Rode, T. and Slabu, I., **2019**. Towards optimized MRI contrast agents for implant engineering: Clustering and immobilization effects of magnetic nanoparticles. *Journal of Magnetism and Magnetic Materials*, 471, pp.432–438.
25. Namvar, F., Rahman, H.S., Mohamad, R., Baharara, J., Mahdavi, M., Amini, E., Chartrand, M.S. and Yeap, S.K., **2014**. Cytotoxic effect of magnetic iron oxide nanoparticles synthesized via seaweed aqueous extract. *International Journal Nanomedicine*, 9, pp.2479–2488.
26. Oanh, V.T.K., Lam, T.D., Thu, V.T., Nam, P.H. and Phuc, N.X., **2016**. A novel route for preparing highly stable Fe₃O₄ fluid with poly (acrylic acid) as phase transfer ligand. *Journal Electronic Materials*, 45(8), pp.4010–4017.
27. Park, Y.C., Smith, J.B., Pham, T., Whitaker, R.D., Sucato, C.A., Hamilton, J.A., Bartolak-Suki, E. and Wong, J.Y., **2014**. Effect of PEG molecular weight on stability, T2 contrast, cytotoxicity, and cellular uptake of superparamagnetic iron oxide nanoparticles (SPIONs). *Colloids Surfaces B:Biointerfaces*, 119, pp.106–114.
28. Parsian, M., Unsoy, G., Mutlu, P., Yalcin, S., Tezcaner, A. and Gunduz, U., **2016**. Loading of Gemcitabine on chitosan magnetic nanoparticles increases the anti-cancer efficacy of the drug. *European Journal of Pharmacology*, 784, pp.121–128.
29. Patil, R.M., Thorat, N.D., Shete, P.B., Bedge, P.A., Gavde, S., Joshi, M.G., Tofail, S.A. and Bohara, R.A., **2018**. Comprehensive cytotoxicity studies of superparamagnetic iron oxide nanoparticles. *Biochemistry and Biophysics Reports*, 13, pp.63–72. [DOI: 10.1016/j.bbrep.2018.07.006](https://doi.org/10.1016/j.bbrep.2018.07.006)
30. Petri-Fink, A., Chastellain, M., Juillerat-Jeanneret, L., Ferrari, A. and Hofmann, H., **2005**. Development of functionalized superparamagnetic iron oxide nanoparticles for interaction with human cancer cells. *Biomaterials*, 26(15), pp.2685–2694.
31. Qi, L. and Xu, Z., **2006**. In vivo antitumor activity of chitosan nanoparticles. *Bioorganic and Medicinal Chemistry Letters*, 16(16), pp.4243–4245.
32. Reimer, P. and Balzer, T., **2003**. Ferucarbotran (Resovist): A new clinically approved RES-specific contrast agent for contrast-enhanced MRI of the liver: Properties, clinical development, and applications. *Eur Radiol*, 13, pp.1266–1276.
33. Robinson, I., Ung, D., Tan, B., Long, J., Cooper, A.I., Fernig, D.G. and Thanh, N.T.K., **2008**. Size and shape control for water-soluble magnetic cobalt nanoparticles using polymer ligands. *Journal of Materials Chemistry*, 18(21), pp.2453–2458.
34. Rohrer, M., Bauer, H., Mintorovitch, J., Requardt, M. and Weinmann, H.-J., **2005**. Comparison of magnetic properties of MRI contrast media solutions at different magnetic field strengths. *Investigative Radiology*, 40(11), pp.715–724.
35. Rosenblum, L.T., Kosaka, N., Mitsunaga, M., Choyke, P.L. and Kobayashi, H., **2010**. In vivo molecular imaging using nanomaterials: General in vivo characteristics of nano-sized reagents and applications for cancer diagnosis. *Molecular Membrane Biology*, 27(7), pp.274–285.
36. Sadeghiani, N., Barbosa, L., Silva, L., Azevedo, R., Morais, P. and Lacava, Z., **2005**. Genotoxicity and inflammatory investigation in mice treated with magnetite nanoparticles surface coated with polyaspartic acid. *Journal of Magnetism and Magnetic Materials*, 289, pp.466–468.
37. Shukla, S., Jadaun, A., Arora, V., Sinha, R.K., Biyani, N. and Jain, V., **2015**. In vitro toxicity assessment of chitosan oligosaccharide coated iron oxide nanoparticles. *Toxicology Reports*, 2, pp.27–39.
38. Silva, A.H., Lima Jr., E., Mansilla, M.V., Zysler, R.D., Troiani, H., Piscioti, M.L.M., Locatelli, C., Benech, J.C., Oddone, N. and Zoldan, V.C., **2016**. Superparamagnetic iron-oxide nanoparticles mPEG350- and mPEG2000-coated: Cell uptake and biocompatibility evaluation. *Nanomedicine: Nanotechnology, Biology and Medicine*, 12(4), pp.909–919.
39. Le, T.T., Du, N.H., Lam, T.D., Tuyet, P.T.H. and Nhan, L.T., **2016**. Study on some factors of magnetic fluid chitosan-coated Fe₃O₄ nanoparticles fabrication via hydrothermal method. *Vietnam Journal of Science and Technology*, 54(2C), pp.341–347.
40. Vuong, T.K.O., Le, T.L., Pham, D.V., Pham, H.N., Ngo, T.H.L., Do, H.M. and Nguyen, X.P., **2015**. Synthesis of high-magnetization and monodisperse Fe₃O₄ nanoparticles via thermal decomposition. *Materials Chemistry and Physics*, 163, pp.537–544.
41. Wei, H., Bruns, O.T., Chen, O. and Bawendi, M.G., **2016**. Nanoparticles for magnetic resonance imaging applications. Google Patents, W02016077769A1.
42. Yang, J., Lee, T.-I., Lee, J., Lim, E.-K., Hyung, W., Lee, C.-H., Song, Y.J., Suh, J.-S., Yoon, H.-G. and Huh, Y.-M., **2007**. Synthesis of ultrasensitive magnetic resonance contrast agents for cancer imaging using PEG-fatty acid. *Chemistry of Materials*, 19(16), pp.3870–3876.
43. Zhang, S., Zhang, Y., Liu, J., Xu, Q., Xiao, H., Wang, X., Xu, H. and Zhou, J., **2013**. Thiol modified Fe₃O₄@ SiO₂ as a robust, high effective, and recycling magnetic sorbent for mercury removal. *Chemical Engineering Journal*, 226, pp.30–38.

Received: 13 August 2019. Accepted: 23 October 2019.